Using Three-Dimensional Spectral/Spatial Gabor Filters for Hyperspectral Region Classification

Tien C. Bau , Subhadip Sarkar and Glenn Healey
Computer Vision Laboratory
Department of Electrical Engineering and Computer Science
University of California, Irvine, CA 92697

ABSTRACT

A 3-D spectral/spatial DFT represents an image region using a dense sampling in the frequency domain. An alternative approach is to represent a 3-D DFT by its projection onto a set of functions that capture specific orientation, scale, and spectral attributes of the image data. For this purpose, we have developed a new model for spectral/spatial information in images based on three-dimensional Gabor filters. This model achieves optimal joint localization in space and frequency and provides an efficient means of sampling a three-dimensional frequency domain representation of HSI data. Since 3-D Gabor filters allow for a large number of spectral/spatial quantities to be used to represent an image region, the performance and efficiency of algorithms that use this representation can be improved if methods are available to reduce the dimensionality of the model. Thus, we have derived methods for selecting filters that emphasize the most significant spectral/spatial differences between the various classes in a scene. We demonstrate the utility of the new model for region classification in AVIRIS data.

Keywords: hyperspectral, texture, recognition, Gabor filterbank

1. INTRODUCTION

Texture modeling is useful in many contexts such as terrain classification and object detection. Several different approaches for modeling multispectral textures can be found in literature. These include the use of multispectral correlation functions[1], Markov Random Fields[2], and fractals[3]. Recognition of hyperspectral textures has also been studied[4,5,6]. Hyperspectral sensors produce images with a large number of spectral bands. Since the pixels in a hyperspectral image contain a large amount of spectral data for a pixel, smaller region sizes might be used for texture recognition. This is especially relevant for remotely sensed imagery where target regions often occupy only a small number of pixels. Due to the large amount of data contained in a hyperspectral image, many current algorithms reduce the dimensionality of the image data using various techniques such as Principal Components Analysis[4] and spectral binning[6]. We employ a combined spectral/spatial representation for hyperspectral data that can effectively exploit spatial as well as spectral correlations within a hyperspectral image.

Gabor filters have received considerable attention in image processing. The Gabor functions achieve optimal joint localization in the original and transform domains[7]. The Gabor functions are also closely related to the human visual system and texture interpretation[7, 8]. Gabor filters can be used to extract components corresponding to different scales and orientations from images. 2D Gabor filters have been used for texture segmentation[9,10], texture analysis[11] and color texture recognition[12]. Gabor filters have also been applied to hyperspectral images using a multiscale opponent representation[6]. 3D Gabor filters have been used to detect motion[13] and to extract and track MRI tagging sheets[14]. We design a 3D Gabor filterbank to extract spectral/spatial components with different orientations and scales using the 3D representation of a hyperspectral image. The output of the Gabor filterbank defines a set of features that describe an image region. We also design a feature selection process that selects the features that emphasize the most significant spectral/spatial differences among a set of classes. This reduced set of optimal features is used for region classification.

2. 3D GABOR FILTERS

A Gabor filter is a sinusoidal function modulated by a Gaussian envelope. A 3D spectral/spatial Gabor filter is defined in the radiance domain by

Algorithms and Technologies for Multispectral, Hyperspectral, and Ultraspectral Imagery XIV, edited by Sylvia S. Shen, Paul E. Lewis, Proc. of SPIE Vol. 6966, 69660E, (2008) · 0277-786X/08/$18 · doi: 10.1117/12.777737

$$g(x,y,\lambda) = a(x,y,\lambda)c(x,y,\lambda) \tag{1}$$

where

$$a(x,y,\lambda) = \frac{1}{(2\pi)^{3/2}\sigma_x\sigma_y\sigma_\lambda} e^{-0.5\left(\frac{x^2}{\sigma_x^2}+\frac{y^2}{\sigma_y^2}+\frac{\lambda^2}{\sigma_\lambda^2}\right)} \tag{2}$$

is the Gaussian component and

$$c(x,y,\lambda) = \cos\left(2\pi\left(F_x x + F_y y + F_\lambda \lambda\right)\right) \tag{3}$$

is the sinusoidal component. The variables, x and y are the spatial variables and λ is the spectral variable. The standard deviations ($\sigma_x,\sigma_y,\sigma_\lambda$) in (2) describe the size of the Gaussian envelope and define the scale of the filter along the spatial and spectral axes. Note that σ_x, σ_y and σ_λ need not be equal and thus the shape of the Gaussian envelope can be ellipsoidal. (F_x,F_y,F_λ) represents the frequency of the sinusoidal component and thus the center frequency of the filter in the 3D frequency domain. The orientation of the filter is defined as the unit vector from the origin to the center frequency (F_x,F_y,F_λ) of the filter. Thus, the orientation of a filter with center frequency (F_x,F_y,F_λ) is given by

$$(\phi_x,\phi_y,\phi_\lambda) = \frac{1}{\sqrt{F_x^2+F_y^2+F_\lambda^2}}\left(F_x,F_y,F_\lambda\right) \tag{4}$$

Due to the symmetry of the filter in the frequency domain, the orientations ($\phi_x,\phi_y,\phi_\lambda$) and ($-\phi_x,-\phi_y,-\phi_\lambda$) are equivalent. Figure 1 depicts a single 3D Gabor filter with orientation (1,0,0) as viewed from three different angles in the radiance domain. The light and dark areas represent positive and negative values of the filter respectively. The half peak bandwidth of the filter in the frequency domain is shown in Figure 2. Since the standard deviations of a Gaussian function in the radiance and frequency domain are inversely proportional, the half peak bandwidth of a filter decreases as the scale increases.

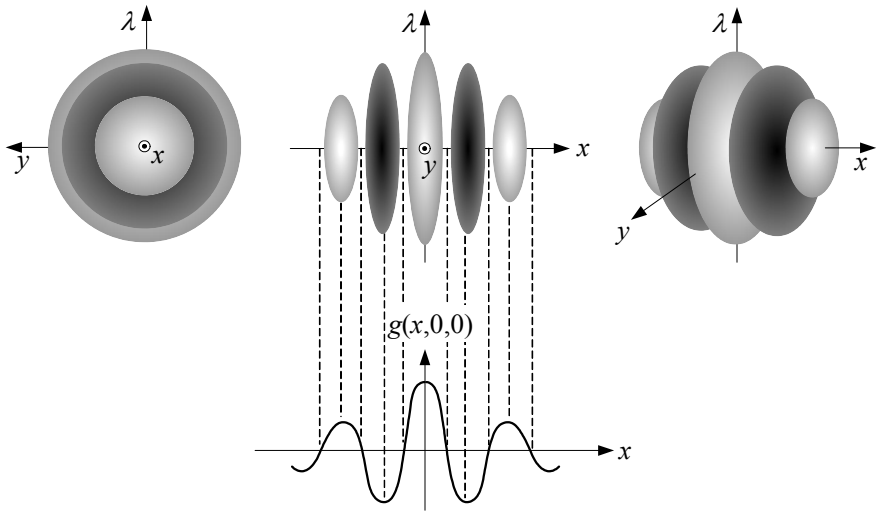

Figure 1. 3D Gabor filter viewed from 3 different angles

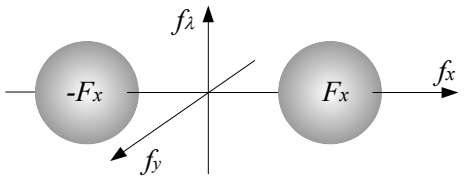

Figure 2. Frequency response of the x-oriented 3D Gabor filter

3. FILTERBANK IMPLEMENTATION

A bank of filters can be constructed to fill the 3D frequency domain by varying both the center frequency (F_x,F_y,F_λ) in (3) and the scales $(\sigma_x,\sigma_y,\sigma_\lambda)$ in (2). Higher frequency filters typically require smaller spatial support and thus have a larger half peak bandwidth in the frequency domain. Filters are often placed one octave apart so that adjacent filters with the same orientation have center frequencies differing by a factor of two[9,12]. As an example, we trace the construction of a filterbank in the frequency domain with five different scales. We construct our filterbank by first generating a set of 3D Gabor filters that have center frequencies $(F_x,0,F_\lambda)$ on the f_x-f_λ plane as shown in Figure 3(a). We consider a set of filters in the f_x-f_λ plane with four distinct orientations giving an angular separation of 45 degrees between adjacent orientations to give a set of 20 filters with center frequencies on the f_x-f_λ plane. Each filter in Figure 3(a) is represented by two ellipsoids showing the half peak bandwidth of the filter. Filters with equal orientation have their center frequencies on the same vector from the origin. For a given orientation, the center frequency of the filter increases and the scale decreases as we move radially outward from the origin. We now rotate and replicate this set of filters in 45 degree steps about the f_λ axis to obtain the complete 3D filterbank. The process is illustrated by Figure 3 and yields a filterbank with 65 filters defined along 13 orientations as shown in Figure 3(c). Only the filters with the largest half peak bandwidth are visible in Figure 3(c). The corresponding radiance domain Gabor filters for a single scale and thirteen different orientations are shown in Figure 4. Each filter in the figure is labeled by its corresponding orientation as defined by (4). For our filterbank, the five scales $(\sigma_x,\sigma_y,\sigma_\lambda)$ are (1.40,1.40,1.40) (2.81,2.81,2.81) (2.81,2.81,5.62) (2.81,2.81,11.23) (2.81,2.81,22.47). We truncate filters at 1.5 cosine cycles in the radiance domain so that the final filter sizes are (5x5x5), (9x9x9), (9x9x17), (9x9x33) and (9x9x65) pixels respectively. We consider one additional filter that measures the DC component. Thus, the total number of filters in our filterbank is 66. All filters are normalized to have unit gain.

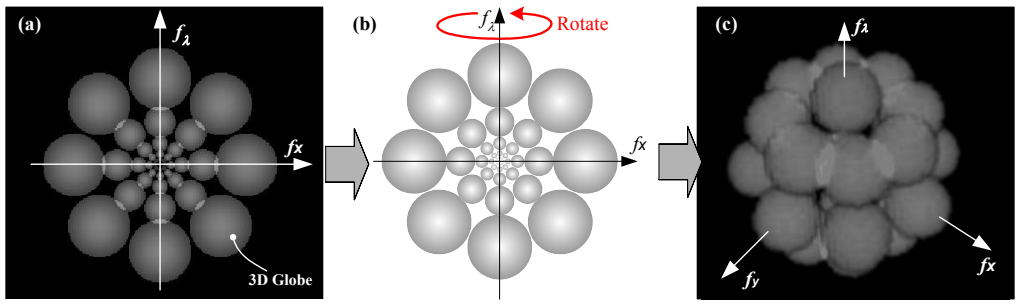

Figure 3. Gabor filterbank in the frequency domain. (a) 3D bank in f_x-f_λ plane. (b) f_x-f_λ plane is rotated to obtain full 3D Gabor filterbank. (c) The resulting 3D Gabor filterbank in the frequency domain.

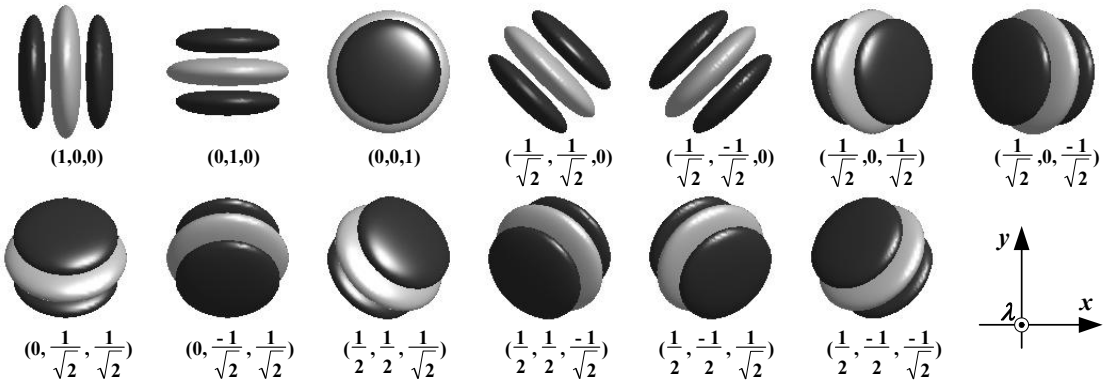

Figure 4. Gabor filters for a single scale and 13 orientations.

4. EXPERIMENTS

4.1 Dataset

We use AVIRIS (Airborne Visible/Infrared Imaging Spectrometer)[15] hyperspectral data for our experiment. This 5m/pixel radiance data was acquired over Pocomoke City, Maryland in 1996 from 20,000 feet altitude. A single band image is shown in Figure 5. The size of the Hyperspectral image is 512x3689 pixels and the 224 bands correspond to wavelengths ranging from 370nm to 2507nm. All 224 bands are used in our experiment. From the image, we obtain a total of 772 sample regions of size 12x12 pixels of the following 11 classes : crop1, crop2, field1, pond, barren1, sand1, veg1, veg2, veg3, weed1 and ClassX. Typical samples for each class (except ClassX) are displayed in Figure 6. ClassX includes samples that are taken from a variety of regions in the image that don't correspond to any of the other ten classes. Half of the 772 samples (386) are used for model training while the other half (386) are used for testing the classification algorithm. Within each dataset (training or testing) of 386 samples, 213 samples belong to 10 classes and 173 samples are from ClassX.

Figure 5. AVIRIS image

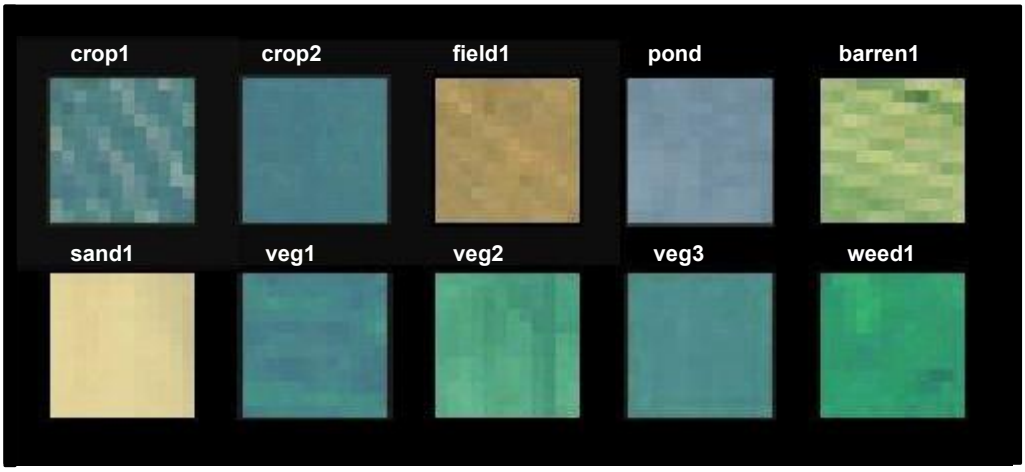

Figure 6. Typical samples from 10 classes

4.2 Features

Each 12x12 region is represented by a combination of spectral and Gabor features. The 224-dimensional mean spectral vector is used to represent a region's spectral properties. Figure 7 plots the mean spectral vectors for typical samples from the 10 specific classes. Let $r_i(x,y,\lambda)$ be the result of filtering a region R with 3D Gabor filter i. The i-th Gabor feature for R is defined by the energy

$$e_R(i) = \frac{1}{x_m y_m \lambda_m} \sum_{x=1}^{x_m} \sum_{y=1}^{y_m} \sum_{\lambda=1}^{\lambda_m} r_i(x,y,\lambda)^2 \qquad (5)$$

where x_m, y_m and λ_m denote the maximum values of x,y and λ in $r_i(x,y,\lambda)$ respectively.

Using the 66 previously defined 3D Gabor filters, we can compute a vector of 66 Gabor features for each region. Figure 8 plots the Gabor feature vector for a typical sample of each of the 10 specific classes.

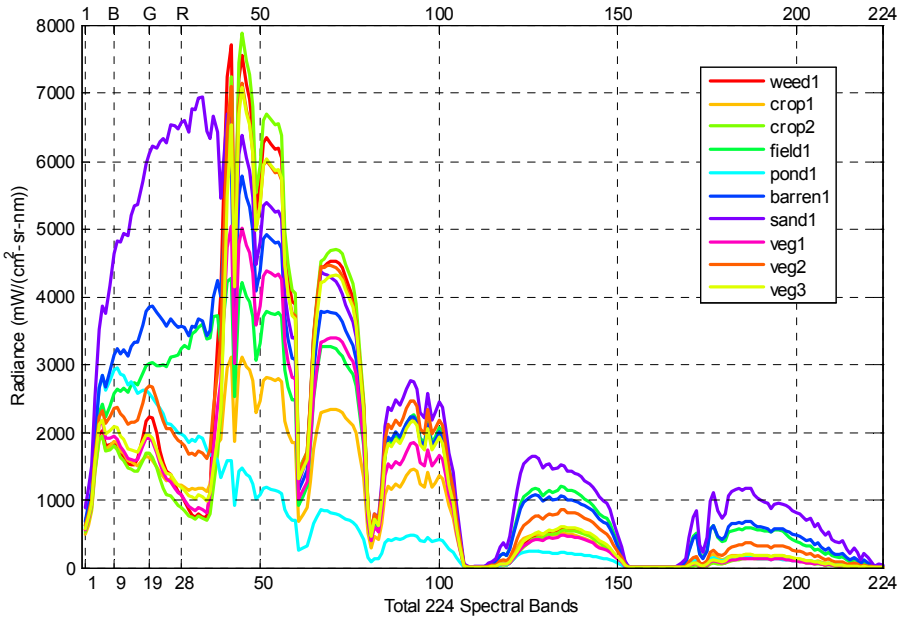

Figure 7. Mean spectral vectors for typical samples from 10 classes

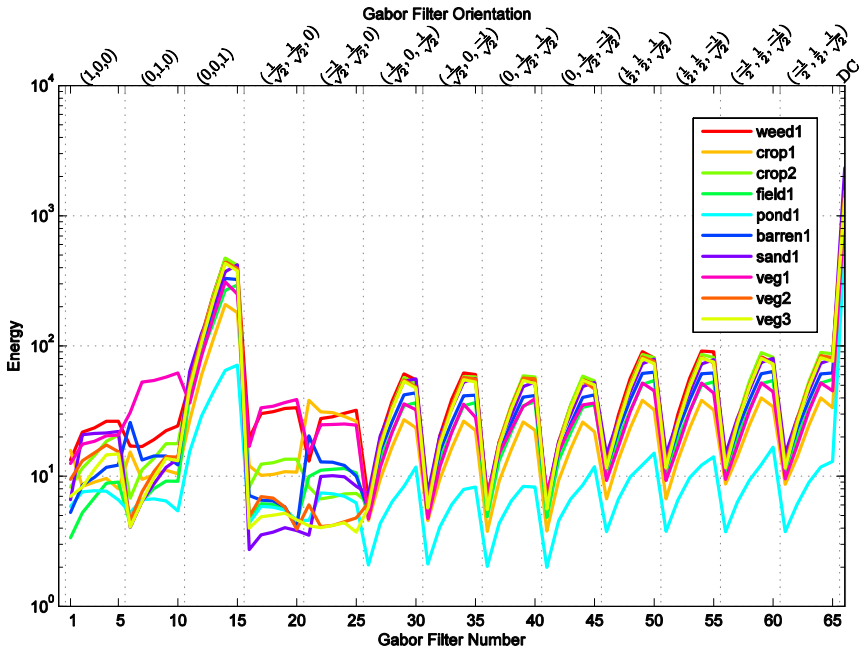

Figure 8. Gabor vectors for typical samples from 10 classes

4.3 Model Training

The goal of model training is to find a subset of features that maximize the classification rate for the samples in the training data. We model the feature vectors for the samples in a class c as normally distributed with mean vector μ_c and covariance matrix Σ_c. As a measure of the likelihood that a sample s is in class c, we use the Mahalanobis distance[16]

$$M(s,c) = \sqrt{(x_s - \mu_c)^T \Sigma_c^{-1} (x_s - \mu_c)} \tag{6}$$

where $x_s = (e_s(1), e_s(2), ..., e_s(D))^T$ is the feature vector for sample *s,* and *D* is the number of features.

For a diagonal covariance matrix Σ_c, equation (6) can be written as

$$M(s,c) = \sqrt{\sum_{i=1}^{D} \left(\frac{x_s(i) - \mu_c(i)}{\sigma_c(i)} \right)^2} \tag{7}$$

where $\mu_c(i)$ is the *i*-th element of μ_c and $\sigma_c(i)$ is the standard deviation of feature $x(i)$ for class *c*. A sample *s* is classified as an instance of the class *c* for which $M(s,c)$ is the smallest.

If a sample *s* has a large Mahalanobis distance with each of the ten specific classes *c*, then *s* should be classified as unknown. Thus, a threshold must be chosen for this purpose. A classical method of defining this threshold is quantile of chi-square distribution, i.e., the percentage of distribution mass enclosed by the threshold contour. If a sample *s* has a Mahalanobis distance that for each of the ten specific classes *c* lies outside the Mahalanobis distance contour that encloses 99% of the distribution for *c* then *s* is classified as unknown.

An optimized feature set is selected using a stepwise optimal algorithm. This algorithm selects a first feature that gives the best classification rate over the 213 training samples associated with the predefined classes. Then we add a new feature from the remaining features that leads to a maximum increase in the classification rate. The algorithm continues by adding new features in this way to maximize the classification rate. The optimum number of features (D') can be determined as the number that gives the highest classification rate.

4.4 Classification Method

After training, the Gaussian model and optimized features can be used for the classification of test data. For an unknown sample, the Mahalanobis distance between the sample's feature vector and the mean vector μ_c for each of the ten predefined classes is calculated using (7). If *s* falls outside of the 99% quantile for each of the predefined classes, then *s* is classified as unknown. Otherwise *s* is classified as an instance of the class with which it has the smallest Mahalanobis distance.

4.5 Classification Results

Figures 9 and 10 plot the classification results for the training and testing datasets. The plots are summarized in Table 1. As a comparison, results for an experiment that uses all of the features for the classification of the training and test data are also provided. We see that combining spectral and Gabor features during classification yields improved results over using spectral or Gabor features in isolation.

Table 1. Classification results for training and test data.

Experiment	Optimized Feature Sets			All Features		
Vector type	Train	D'	Test	Train Data	D	Test Data
Spectral	83%	24	82%	77%	224	79%
Gabor	93%	8	90%	84%	66	83%
Spectral+Gabor	98%	7	95%	85%	290	85%

An analysis of the experiment reveals some interesting characteristics of the features. Spectral features will often misclassify a region with the same materials mixed in the same ratio as a model class even if the region has different spatial properties than the model class. In Figure 11(a), the image on the right is a typical crop1 sample, while the image on the left (sample_1) is a ClassX sample. Despite the difference in the spatial structure, sample_1 is misclassified as crop1 when using spectral features. The two regions have similar mean spectral vectors as shown in Figure 12. This sample_1, however, can be correctly distinguished by using Gabor features as shown in Figure 13. The Gabor features for crop1 at orientation $(-1/\sqrt{2}, 1/\sqrt{2}, 0)$ have much greater energy than those in sample_1. By contrast, sample_1 has more energy in the (1,0,0), (0,1,0) and $(1/\sqrt{2}, 1/\sqrt{2}, 0)$ directions which indicates a more isotropic texture structure. The result of the stepwise feature selection process confirms that Gabor filters #1, #6, #16 and #21, are crucial for distinguishing

sample_1 from the crop1 class. A similar situation occurs for the samples shown in Figure 11 (b),(c) and (d). Each of these cases are misclassified using spectral features but are classified correctly using Gabor features.

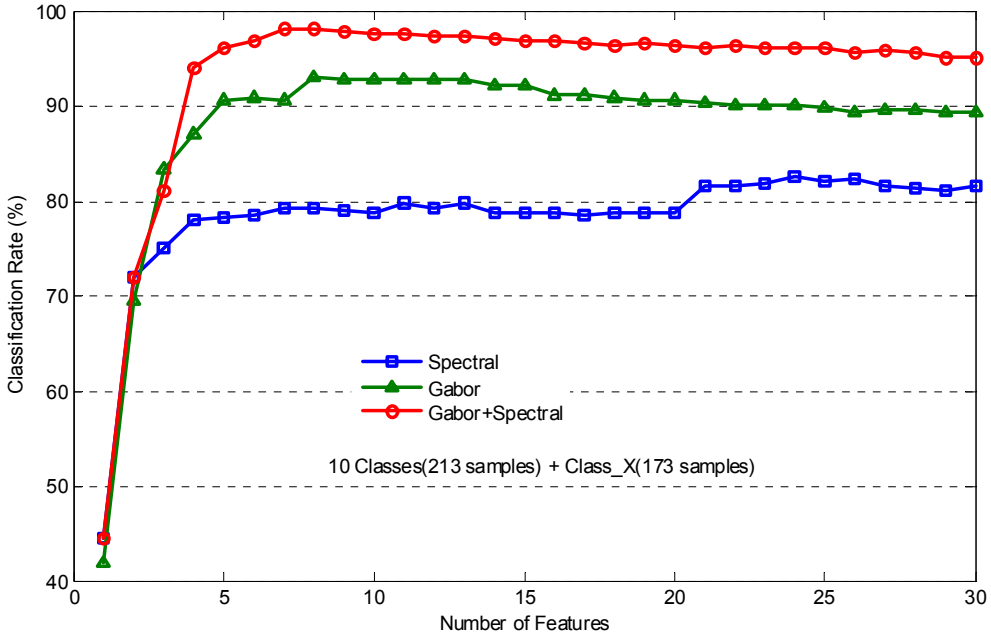

Figure 9. Classification of training data

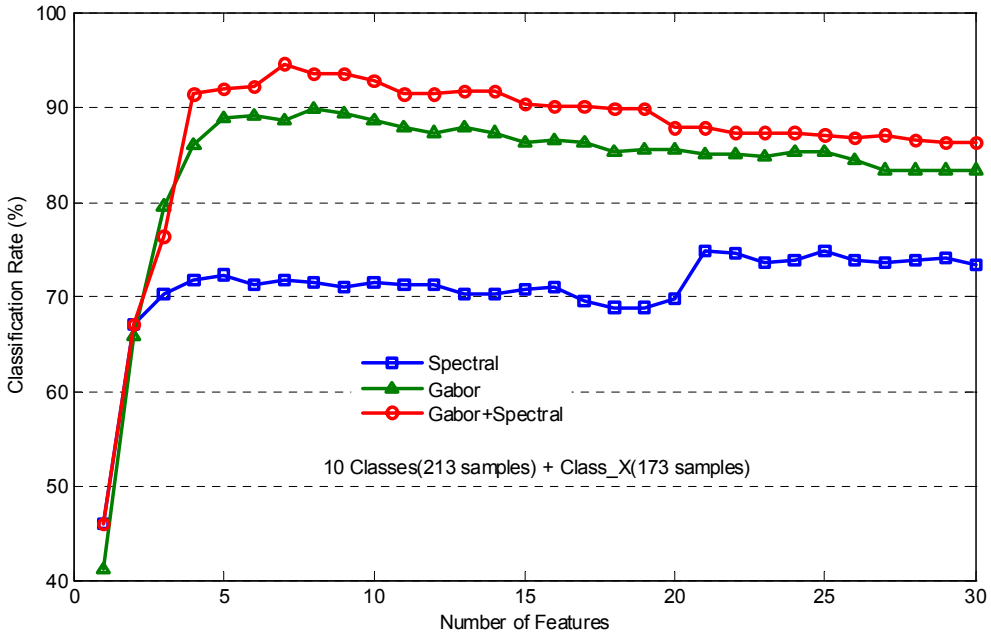

Figure 10. Classification of test data

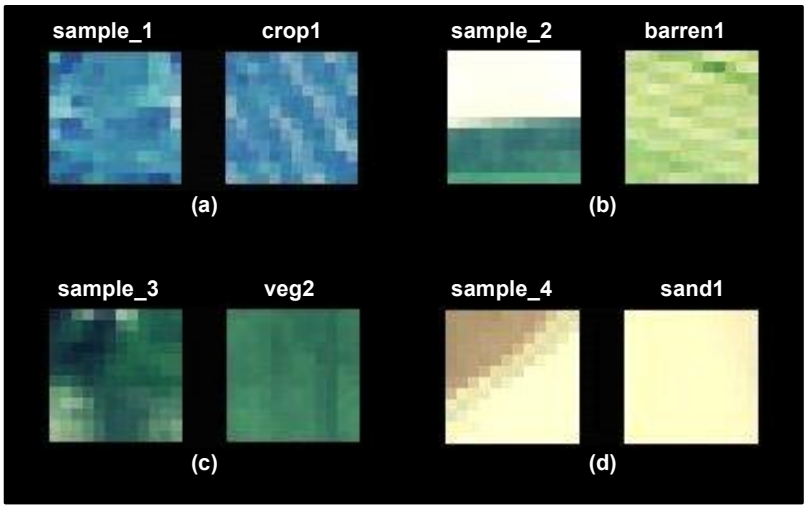

Figure 11. Examples of misclassified sample pairs using only spectral features. Samples on the left of a pair are ClassX samples.

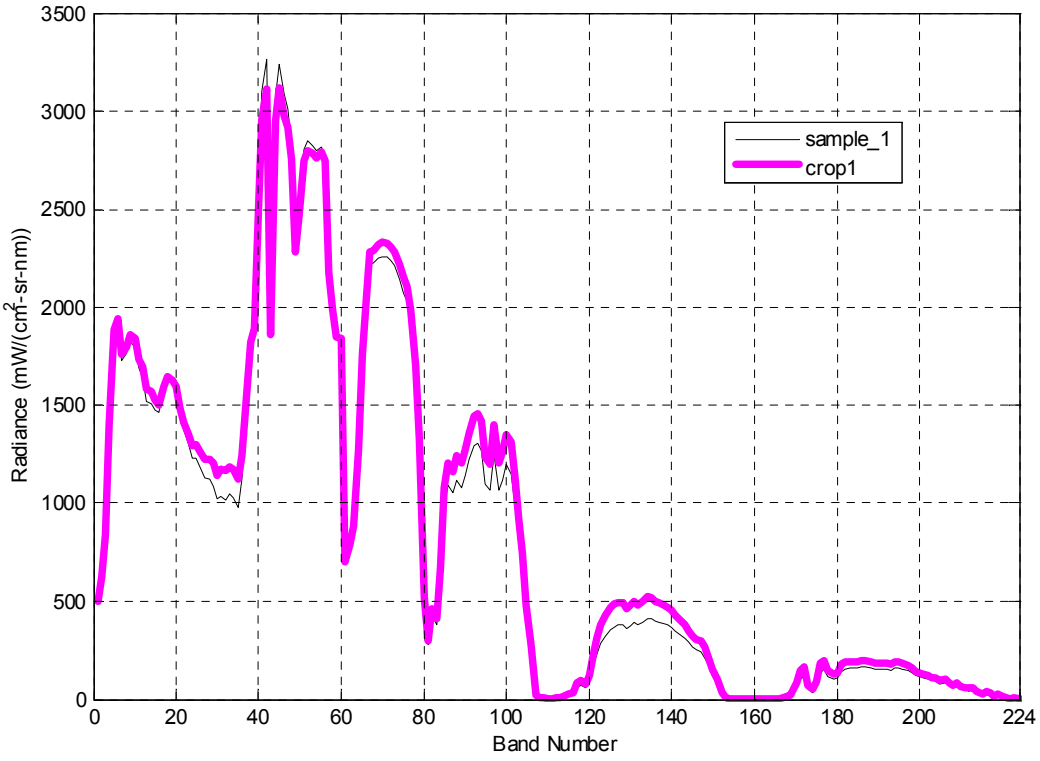

Figure 12. Spectral mean vector for ClassX sample and crop1 sample in Figure 11(a)

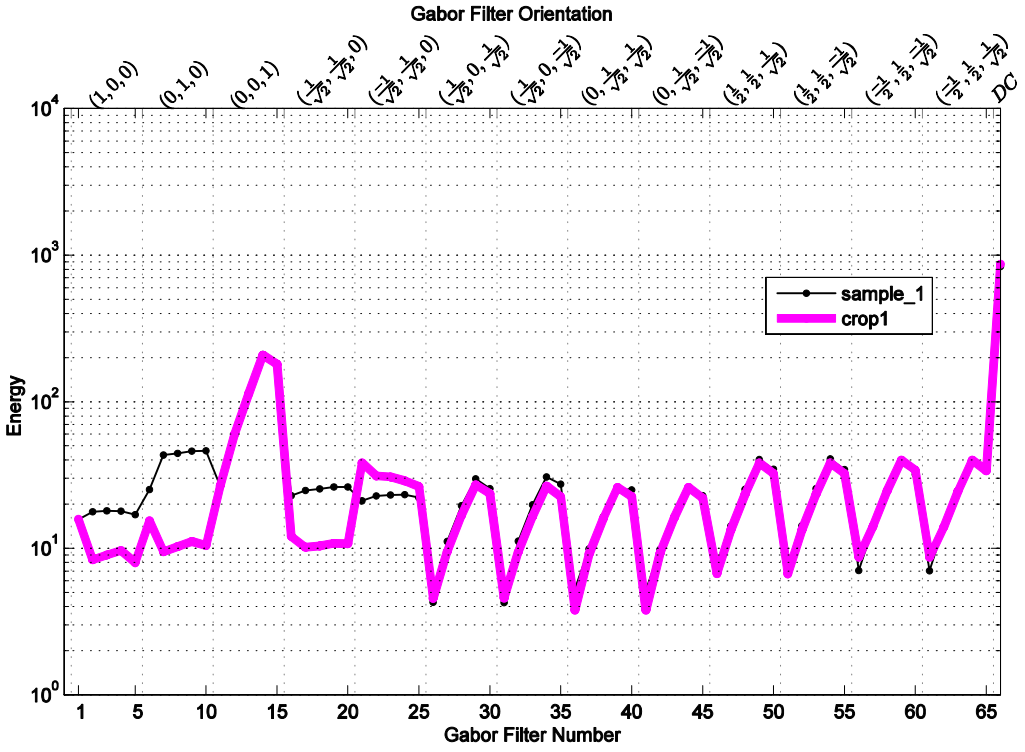

Figure 13. Gabor vector for sample_1 and crop1 in Figure 11(a).

There are also situations where the Gabor features in isolation are not sufficient to correctly classify a sample. Figure 14(a) shows sample_5 along with another sample from the class barren1. However, sample_5 lies outside the 99% contour for class barren1 due to minor texture differences. Figure 14(b) shows sample_6 along with another sample from the class field1. The region sample_6 lies outside the 99% contour for class field1 due to small differences in spatial structure. Both sample_5 and sample_6 are correctly classified if spectral features are utilized.

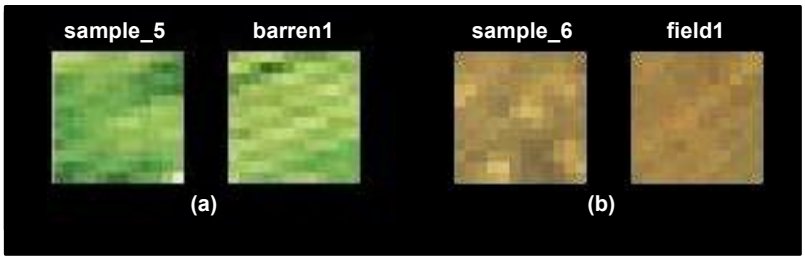

Figure 14. Examples of misclassified samples when using only Gabor features.

We see from figures 9 and 10 that the best classification results are achieved by using a combination of spectral and Gabor features. The first seven features chosen by the stepwise optimal algorithm in order of importance are 176S, 5S, 29G, 16G, 1G, 55G, 6G where S indicates a spectral feature and G indicates a Gabor feature. Three of the five Gabor features #1 (1,0,0), #6 (0,1,0), and #16 ($1/\sqrt{2}, 1/\sqrt{2}, 0$) are without wavelength dependence while the two filters #29 ($1/\sqrt{2}, 0, 1/\sqrt{2}$) and #55 ($1/2, 1/2, -1/\sqrt{2}$) measure spatial/spectral dependence. Feature #29, for example, measures correlation between x and λ. Figures 15 and 16 show samples that have similar spectral properties but significantly different values for feature #29.

5. SUMMARY AND CONCLUSION

We have presented an algorithm for hyperspectral region classification by using 3D spectral/spatial Gabor features. We designed a 3D Gabor filterbank capable of capturing the energy of spectral/spatial texture at different orientations and scales. Three different combinations of feature vectors (Spectral, Gabor, and Spectral+Gabor) were tested in classification experiments. The results show that the 3D Gabor features successfully separate samples with similar material composition but different texture structure. We have also demonstrated why the 3D Gabor spectral/spatial features can be important in the feature selection process. The combined spectral and 3D Gabor features are shown to be effective for hyperspectral region classification.

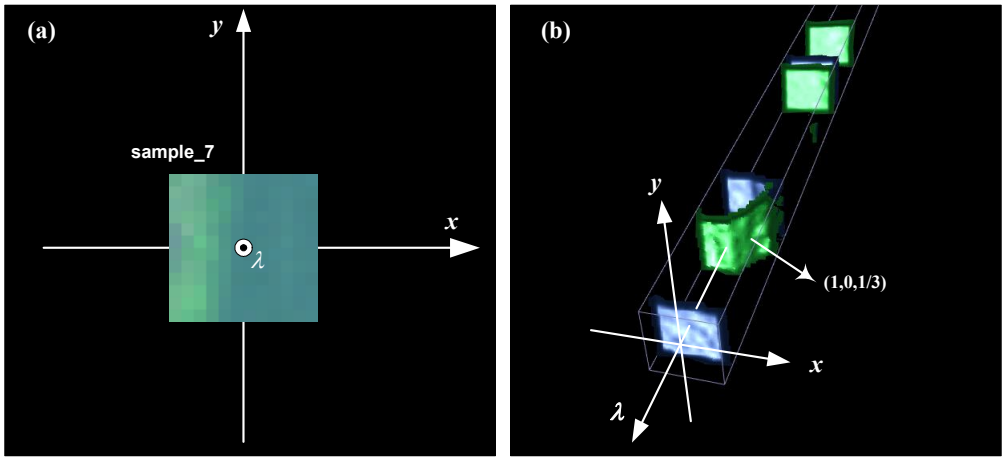

Figure 15. Sample that has energy captured by filter #29. Single-band view (a) and 3D iso-surface view (b).

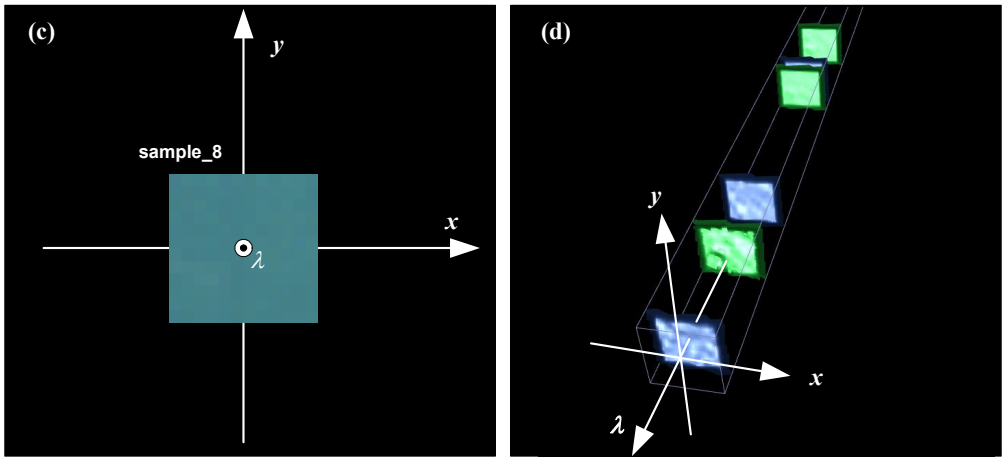

Figure 16. Sample that has little energy captured by filter #29. Single-band view (c) and 3D iso-surface view (d)

REFERENCES

1. P. Suen and G. Healey, "The analysis and recognition of real-world textures in three dimensions," *IEEE Trans. Pattern Anal. Mach. Intell*. 22(5),491-503, 2000.
2. J. Bennett and A. Khotanzad, "Multispectral random field models for synthesis and analysis of color images," *IEEE Trans. Pattern Anal. Mach. Intell.* 20(3), 327-332, 1998.
3. S. E. Franklin, R. J. Hall, L. M. Moskal, A. J. Maudie, and M. B. Lavigne, "Incorporating texture into classification of forest species composition from airborne multispectral images," *Int. J. Remote Sensing* 21(1), 61-79, 2000.
4. S. Sarkar and G. Healey, "Hyperspectral texture classification using generalized Markov fields," *Optical Engineering* 43(12), 3038-3044, 2004.

5. X. Zhang, N. H. Younan, and C. G. O'Hara, "Wavelet domain statistical hyperspectral soil texture classification," *IEEE Trans. Geosci. Remote Sens.* 43(3), 615-618, 2005.
6. M. Shi and G. Healey, "Hyperspectral texture recognition using a multiscale opponent representation," *IEEE Trans. Geosci. Remote Sens.* 41(5), 1090-1095, 2003.
7. J. G. Daugman, "Uncertainty relation for resolution in space, spatial frequency, and orientation optimized by two-dimensional visual cortical filters," *J. Opt. Soc. Am*. A 2(7), 1160-1169, 1985.
8. D. A. Clausi and M. E. Jernigan, "Designing Gabor filters for optimal texture separability," *Pattern Recognition* 33(11), 1835-1849, 2000.
9. A. K. Jain and F. Farrokhnia, "Unsupervised texture segmentation using Gabor filters," *Pattern Recognition* 24(12), 1167-1186, 1991.
10. T. Weldon and W. E. Higgins, "Designing multiple Gabor filters for multitexture image segmentation," *Optical Engineering* 38(9), 1478-1489, 1999.
11. A. C. Bovic, M. Clark, and W. S. Geisler, "Multichannel texture analysis using localized spatial filters," *IEEE Trans. Pattern Anal. Mach. Intell.* 12(1), 55-73, 1990.
12. A. Jain and G. Healey, "A multiscale representation including opponent color features for texture recognition," *IEEE Trans. Image Process.* 7(1), 124-128, 1998.
13. T. R. Reed, "On the computation of optical flow using the 3-d Gabor transform, "*Multidimensional Systems and Signal Processing* 9(4), 447-452, 1998.
14. Z. Qian, D. N. Metaxas, and L. Axel, "Extraction and tracking of MRI tagging sheets using a 3d Gabor filter bank," in *IEEE conf. on Engineering in Medicine and Biology Society*, 711-714, 2006.
15. G. Vane, R.Green, T. Chrien, H. Enmark, E. Hansen, and W. Porter, "The airborne visible/infrared imaging spectrometer (AVIRIS)," Remote Sensing of the Environment 44, pp. 127-143, 1993.
16. R. O. Duda, P. E. Hart, and D. G. Stork, Pattern Classification, 2nd ed., Wiley, New York, 2001.